Spin-resolved atomic orbital model refinement for combined charge and spin density analysis: application to the YTiO 3 perovskite

Iurii Kibalin, Ariste Bolivard Voufack, Mohamed Souhassou, Béatrice Gillon, Jean-Michel Gillet, Nicolas Claiser, Arsen Gukasov, Florence Porcher, Claude Lecomte

Spin-resolved atomic orbital model refinement for combined charge and spin density analysis: application to the $YTiO_3$ perovskite

Iurii Kibalin[abc], Ariste Bolivard Voufack[bd], Mohamed Souhassou[b]*, Béatrice Gillon[a], Jean-Michel Gillet[e], Nicolas Claiser[b], Arsen Gukasov[a], Florence Porcher[a] and Claude Lecomte[b]

[a]Laboratoire Léon Brillouin, CEA-CNRS, CE-Saclay, Gif-sur-Yvette, 91191, France

[b]CRM2, Institut Jean Barriol, Lorraine University and CNRS, BP239, Vandoeuvre-les-Nancy, F54506, France

[c]PNPI, NRC "Kurchatov Institute", Orlovarosha, Gatchina, Leningrad region, 188300, Russian Federation

[d]MACETS, Faculté des sciences, Université de Dschang, B.P. 67, Dschang, Cameroon

[e]Laboratoire SPMS, UMR 8580, CentraleSupélec, Paris-Saclay University, Gif sur Yvette, 91191, France

Correspondence email: mohamed.souhassou@univ-lorraine.fr

Funding information We thank the ANR (Agence nationale de la recherche) through the MTMED project: multi-techniques modelling of electron densities. IK thanks the ANR for his postdoctoral position. ABV thanks the ANR for financial support.

Synopsis The paper reports on a new crystallographic method to refine a spin-resolved atomic orbital model against X-ray and polarized neutron diffraction data. Radial extension of atomic orbitals, their orientations and populations are obtained for each atom in the $YTiO_3$ perovskite crystal.

Abstract A new crystallographic method is proposed in order to refine a spin-resolved atomic orbital model against X-ray and polarized neutron diffraction data. This atomic orbital model is applied to the $YTiO_3$ perovskite crystal, where orbital ordering has previously been observed by several techniques: X-ray, polarized neutron diffraction and nuclear magnetic resonance. This method gives radial extension, orientation and population of outer atomic orbitals for each atom. The interaction term between Ti^{3+}, Y^{3+} cations and O^{2-} ligands can be estimated. The refinement qualities obtained by means of the orbital is compared to that obtained by multipole models previously published.

Keywords: atomic orbital model; polarized neutrons diffraction; X-ray diffraction; perovskite; spin density; charge density.

1. Introduction

The representation of experimentally derived electron density plays an important role in the characterization of chemical interactions; this density may be described by a set of model parameters or by numerical values on a 3D grid. The former is the most suitable for electrostatic calculations and topological analysis since all properties can be calculated analytically.

The multipole model was developed and widely used for the analysis of charge density distribution measured by X-ray diffraction (XRD) (Bentley & Stewart, 1973; Stewart, 1969; Hansen & Coppens, 1978). It was later extended to spin density (Brown, et al., 1979). In this case, electron density is expressed as a linear combination of spherical harmonics. Such a model has been remarkably successful in estimating various electrostatic physical quantities such as electrostatic fields, electrostatic potentials and electrostatic moments (Jelsch, et al., 2005). When the system possesses magnetic properties, knowledge of the electron spin density distribution is needed. The polarized neutron diffraction (PND) method provides the spin distribution at the atomic scale. A spin-resolved multipole model combining information from XRD and PND experiments was developed in our laboratories and implemented in the ``MOLLYNX'' program (Deutsch, et al., 2012). It has been successfully applied to organic radicals (Voufack, et al., 2017), coordination compounds (Deutsch, et al., 2014) and inorganic perovskites (Voufack, et al., 2019).

However, the multipole model is not suitable for retrieving some fundamental quantities such as first-order density matrices or the orbital representation of wave functions. Nevertheless, the multipole model deduced from charge density analysis does not provide the populations of atomic orbitals, when they are approximately estimated by the Holladay's method (Holladay, et al., 1983). It should be noted that an atomic orbital model refinement was previously developed for spin density analysis only. In this model the atomic wave function is constructed as a linear combination of the atomic orbitals localized on each atom which are supposed to carry unpaired electrons, the populations of which are refined on the basis of the PND data (Schweizer & Ressouche, 2001).

The present model is based on quantum mechanical orbitals, proposed by K. Tanaka for charge density analysis, and provides the aforementioned physical quantities (Tanaka, 1988). Tanaka's model gives access to molecular or atomic orbitals from the structure factors measured by XRD. Nevertheless, the difficulty in implementing this model lies in the refinement of orthogonal wave functions ψ_i defined for each electron in the system. Because the constraint conditions on the parameters of wave functions quadratically increase with the number of electrons, the least-squares refinement usually failed for large amount of non-linear constraints. The problem was circumvented by neglecting overlap between atomic orbitals located on different atoms (Tanaka, et al., 2008) , but it

does not allow a fully quantitative description of the inter-atomic interactions. Figgis and coworkers have also proposed such a model applied for example on a copper complex (Bytheway, et al., 2001).

The objective of the paper is to describe a spin-resolved simplified atomic orbital model where interaction between atoms is accounted for. The model was implemented into our previously developed program ``MOLLYNX'' for joint XRD and PND refinement (Deutsch, et al., 2012). The following sections are considered in the paper: description of the atomic orbital model, calculation of the electron density, XRD and PND structure factors and refinement using non-linear least-squares refinement constraints. Then the validity of this spin-resolved atomic orbital is demonstrated using $YTiO_3$ perovskite's XRD and PND. The refinement quality is compared to that obtained with the spin-resolved multipolar model (Voufack, et al., 2019). The contribution of the different atomic orbitals to the magnetization of the sample is discussed.

2. Atomic orbital model

2.1. Total electron density

In this model, the total electron density $\rho(\vec{r})$ is represented as a sum of two terms: the density of electrons centered on atoms and that lying on the bonds $\rho_b(\vec{r})$. The first term is itself a sum of spherical ``core'' term $\rho_c(\vec{r})$ and non-spherical external ``valence'' terms $\rho_v(\vec{r})$:

$$\rho(\vec{r}) = \rho_c(\vec{r}) + \rho_v(\vec{r}) + \rho_b(\vec{r}). \quad (1)$$

To construct ``core'' terms the radial function $R_i(r)$ for each shell has to be defined with electron populations p_i on the shell i for all A atoms;

$$\rho_c(\vec{r}) = \sum_A \sum_i \frac{1}{4\pi} \cdot p_i \, R_i^2(|\vec{r} - \vec{r}_A|). \quad (2)$$

The radial functions (R_i) implemented into the ``MOLLYNX'' program (Deutsch, et al., 2012) are described in the following subsection. The populations p_i are respectively equal to 2, 6 and 10 for s, p and d full core shells.

The ``valence'' term can be represented through atomic orbitals ϕ_i, which are linear combinations, with c_{iv} coefficients, of orthonormal basis functions χ_v

$$\phi_i = \sum_v c_{iv}\chi_v.$$

Although the orbitals $\{\phi_i\}$ can arbitrarily be defined, orthonormal atomic orbitals are used to reduce the multiplicity in representation of density $\rho_v(\vec{r})$.

The density $\rho_v(\vec{r})$ is the sum over all the square modulus of valence orbitals ϕ_i having population n_i:

$$\rho_v(\vec{r}) = \sum_A \sum_i n_i \sum_{\mu,\nu} c_{i\mu} c_{i\nu} \chi_\mu(\vec{r} - \vec{r}_A) \chi_\nu(\vec{r} - \vec{r}_A). \quad (3)$$

Here A runs over the number of atoms, i over the number of valence atomic orbitals and μ, ν run over basis functions $\{\chi_\mu\}$.

To describe the total electron density, the density $\rho_b(\vec{r})$ of bonded pairs of atomic orbitals $\phi_i$and ϕ_j centered on different interacting atoms A and B is used (two-center orbital product):

$$\rho_b(\vec{r}) = \sum_{A \neq B} \sum_{i,j} \frac{n_{ij}}{N_{ij}} \sum_{\mu,\nu} c_{i\mu} c_{j\nu} \chi_\mu(\vec{r} - \vec{r}_A) \chi_\nu(\vec{r} - \vec{r}_B). \quad (4)$$

The parameter n_{ij} characterizes the electron population of the orbital product $\phi_i \phi_j$. The normalization constant N_{ij} is the orbital overlap: $N_{ij} = \int \phi_i(\vec{r} - \vec{r}_A) \phi_j(\vec{r} - \vec{r}_B) d^3\vec{r}$. Zero constant N_{ij} corresponds to orthogonal orbitals, for which the orbital product cannot be populated. This term is supposed to be large for covalent bonds.

2.2. Basis functions

For hydrogen-like orbitals (s, p, d and so on), the orbital basis functions may be expressed as the product of radial $R_\mu(r)$ and real spherical harmonics $Y_{lm}(\theta, \phi)$ functions:

$$\chi_\mu(r, \theta, \phi) = R_\mu(r) Y_{lm}(\theta, \phi). \quad (5)$$

Several functions have been proposed to describe the radial function (Stewart, 1969; Bonham, 1965; Stewart, et al., 1965). Here we use the following description: according to Clementi (Clementi & Roetti, 1974) the radial function for orbitals of isolated atoms can be expressed as a sum of Slater functions (STO):

$$R_\mu(r) = \sum_{k=1}^{N_{STO}} p_k \frac{(2\zeta_k)^{n_k + 1/2}}{\sqrt{2n_k!}} r^{n_k - 1} e^{-\zeta_k r}. \quad (6)$$

The expansion of the radial part on Gaussian functions is widely used in ab-initio calculations and radial function can also be described via Gaussian type orbitals (GTO). The analytical expression is:

$$R_\mu(r) = \frac{2^{n+3/4} r^{n-1}}{\pi^{1/4} \sqrt{(2n-1)!!}} \sum_{k=1}^{N_{GTO}} p_k \alpha_k^{\frac{2n+1}{4}} e^{-\alpha_k r^2}. \quad (7)$$

GTO have proved to be more convenient for computing two-center integrals than STO and have thus become more popular for many numerical applications.

The parameters p_k, ζ_k, α_k are tabulated values which can be found in handbooks (Clementi & Roetti, 1974; Schuchardt, et al., 2007) for both models for each neutral atom shell.

The extension of atomic orbitals depends on the nature of chemical bonding between neighboring atoms. The radial function can be modified by means of the expansion contraction coefficient κ (called also scaling parameter) which is a multiplying factor of the radius r.

2.3. Spin and charge structure factors

The interpretation of XRD and PND experiments requires an accurate estimation of electronic and magnetic structure factors, which are Fourier transforms of the charge and spin densities, respectively. As the Fourier transform is a linear operation, structure factors can also be separated into ``core" $F_c(\vec{H})$, ``valence" $F_v(\vec{H})$ and ``bond" terms $F_b(\vec{H})$.

The Fourier transform of ``core" electron density is expressed as:

$$F_c(\vec{H}) = \sum_A T_A \left[\sum_i \frac{p_i}{4\pi} \int_0^\infty R_i^2(r) j_0(2\pi Hr) dr + F_A \right], \quad (8)$$

where $j_0(2\pi Hr)$ is a zeroth-order spherical Bessel function. T_A is the Debye-Waller factor of atom A (Shmueli, 2001). The complex value F_A is the anomalous scattering part of atom A in the case of X-rays only. The integral in (8) has an analytical solution when the radial function R_μ is expressed through STO (Avery & Watson, 1977) or GTO orbitals (Chandler & Spackman, 1978).

The ``valence" component of the structure factor includes the contribution from the outer orbitals located on the same atom:

$$F_v(\vec{H}) = \sum_A T_A \sum_i n_i \sum_{\mu,\nu} c_{i\mu} c_{i\nu} \int \chi_\mu \chi_\nu e^{i2\pi \vec{H}\cdot\vec{r}} d^3\vec{r}. \quad (9)$$

The integral $\int \chi_\mu \chi_\nu e^{i2\pi \vec{H}\cdot\vec{r}} d^3\vec{r}$ has a simple analytical solution for STO and GTO orbitals (Stewart, 1969; Tanaka, 1988; Chandler & Spackman, 1978; Shmueli, 2001; Tanaka, et al., 2008). Note that the one-center orbital product can be represented as a radial function multiplied by a sum over spherical harmonic functions weighted by Clebsch-Gordan coefficients. It follows that the modeled density is formally equivalent to the multipole model description extended up to 4th-order spherical functions for the valence shell p, and up to 6th-order spherical functions for the valence shell d.

The ``bond" term describes electrons shared by two neighboring atoms. Therefore, the Fourier transforms of two-center orbital products have to be calculated. If the radial function is expressed through GTO orbitals, the Fourier transform has an analytical expression (Avery & Watson, 1977). Therefore, as the integral solution for STO orbitals is expressed through generalized hypergeometric functions (Niehaus, et al., 2008; Vuković & Dmitrović, 2010), in the present work the ``bond" structure factor is calculated using GTO orbitals which is less complicated that STOs.

Nevertheless, STO orbitals are better suited than GTO orbitals to represent electron wave functions. The expansion over STO orbitals is therefore used for the structure factor calculations of ``core'' and ``valence'' terms, while GTO orbitals are applied only for the ``bond'' term calculations.

X-ray diffraction allows reconstructing the total electron distribution, while polarized neutron diffraction provides information about the spin density, i.e. the unpaired electron distribution. These two quantities can be expressed in terms of spin-resolved populations of atomic orbitals, respectively representing the sum and the difference between spin up $n_i^{\uparrow}$, $n_{ij}^{\uparrow}$ and spin down $n_i^{\downarrow}$, $n_{ij}^{\downarrow}$ populations. The charge and spin structure factors are thus calculated as:

$$F_{charge} = F_c + F_v^{\uparrow} + F_v^{\downarrow} + F_b^{\uparrow} + F_b^{\downarrow}, \tag{10}$$

$$F_{spin} = F_v^{\uparrow} - F_v^{\downarrow} + F_b^{\uparrow} - F_b^{\downarrow}, \tag{11}$$

where each spin-dependent component is calculated using the corresponding spin dependent populations n_i and n_{ij}.

The relations between the corresponding structure factors and the diffraction intensities (in the case of XRD) or flipping ratios (in the case of PND) can be found in the literature (Stewart, et al., 1965; Gillon & Becker, 2011).

2.4. Constraints over model parameters

The described model is fitted against the XRD and PND data by a least-squares refinement procedure. As usual, several constraints must be applied to the refined parameters.

To ensure the electroneutrality of the unit cell, the total number of electrons is required to remain unchanged in the unit cell:

$$\sum_A \sum_i \left(n_i^{\uparrow} + n_i^{\downarrow}\right) + \sum_{A>B} \sum_{i,j} \left(n_{ij}^{\uparrow} + n_{ij}^{\downarrow}\right) = const. \tag{12}$$

A similar constraint concerns the conservation of the magnetic moment, i.e. the number of unpaired electrons in the unit cell. It is written as:

$$\sum_A \sum_i \left(n_i^{\uparrow} - n_i^{\downarrow}\right) + \sum_{A>B} \sum_{i,j} \left(n_{ij}^{\uparrow} - n_{ij}^{\downarrow}\right) = const. \tag{13}$$

The refinement of the orthonormal atomic orbitals $\{\phi_i\}$ leads to additional constraints on the orientation parameters $\{c_{i\mu}\}$:

$$\sum_{\mu} c_{i\mu} c_{j\mu} = \delta_{ij}, \qquad (14)$$

for each pair of orbitals ϕ_i and ϕ_j located on the same atom. δ_{ij} is the Kronecker delta piecewise function. The cross-term $c_{i\mu} c_{j\nu}$ is absent in (14) due to the mutual orthogonality of the orbital basis functions χ_μ and χ_ν.

The electroneutrality and spin constraints are of linear type. There are several methods devoted to the implementation of such constraints in the least-squares refinement procedure (Raymond, 1972; Hamilton, 1964). One of the usual methods in crystallography is the Hamilton method (Hamilton, 1964). In order to introduce non-linear constraints (orthonormal atomic orbitals$\{\phi_i\}$) the classical Hamilton method has been extended. The mathematical description is given in the appendix A.

3. Spin resolved electron density in $YTiO_3$

The performance and validity of this new method is evaluated on the $YTiO_3$ perovskite crystal ; its charge and spin densities are decomposed into “core", ``valence" and ``bond" contributions. Figure 1 shows the structure of $YTiO_3$ (orthorhombic, space group Pnma). The Ti^{3+} ion sits on the center of a centrosymmetric distorted oxygen octahedron. The Y^{3+} ion sits on a mirror plane and is coordinated by eight oxygen atoms forming a distorted square antiprism.

This perovskite was intensively studied by means of various experimental and theoretical methods such as nuclear magnetic resonance (Itoh & Tsuchiya, 2001), polarized (Akimitsu, et al., 2001) and unpolarized (Ulrich, et al., 2002) neutron diffraction, inelastic neutron scattering (Li, et al., 2014), resonant X-ray scattering (Nakao, et al., 2002), soft X-ray linear dichroism (Iga, et al., 2004), X-ray magnetic diffraction (XMD) (Ito, et al., 2004), Compton scattering (Tsuji, et al., 2008) and elastic X-ray scattering (Hester, et al., 1997). Such interest is mainly due to the existence of an antiferromagnetic orbital ordering in the ferromagnetic state of $YTiO_3$(its Curie temperature is 30 K). Theoretical studies using unrestricted Hartree-Fock calculations and density functional theory with generalized gradient approximation predicted the wave function of the 3d electrons of titanium atoms to be a linear combination of $|xz\rangle$ and $|yz\rangle$ orbitals in the t_{2g} state (Mochizuki & Imada, 2004). The experimental estimation of the atomic orbitals orientation from PND and XMD data (Akimitsu, et al., 2001; Ito, et al., 2004; Kibalin, et al., 2017) was performed within the approximation of a single unpaired electron located on the $|3d\rangle$ orbitals of the octahedrally coordinated titanium atom. The results are in good agreement with the theoretical predictions (Kibalin, et al., 2017).

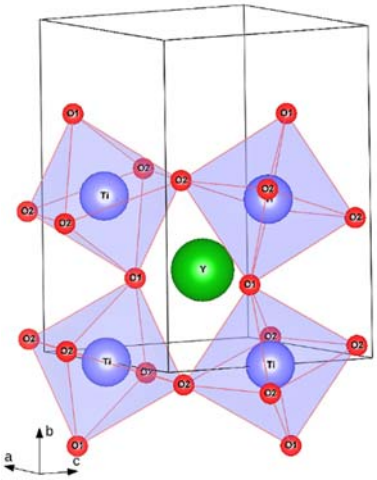

Figure 1 Crystal structure of $YTiO_3$ (orthorhombic, space group Pnma)

In this paper we investigate beyond the limitation of one unpaired electron and take advantage of the spin-resolved atomic orbital model explained above to perform a combined analysis of charge and spin densities.

3.1. Experiments

The charge density analysis was made using synchrotron diffraction data (SPRING8 beamline BL02B2) on a single crystal ($0.021 \times 0.100 \times 0.109$ mm^3) at 20 K in the ferromagnetic phase. A short wavelength (0.353 Å) was used to reduce absorption and extinction effects. The details of experimental conditions are given in our previous paper (Voufack, et al., 2019).

The polarized neutron diffraction measurements were performed at the thermal polarized neutron lifting-counter diffractometer 6T2 and the hot polarized neutron two-axis diffractometer 5C1 (LLB-Orphée, Saclay). The data were obtained at 5 K, in the ferromagnetic phase, under an applied magnetic field of 5 T, respectively parallel to the **a**-, **b**- and **c**-axes of single-crystalline sample, with two neutron wavelengths, 1.4 Å (6T2 diffractometer) and 0.84 Å (5C1 diffractometer). The incomplete beam polarization and extinction effects were corrected for. The details of neutron measurements are provided in (Kibalin, et al., 2017).

3.2. Model parameters

To specify the orbital model, ``core", ``valence" and ``bond" terms have to be defined. The parameters characterizing the ``core" term are not refined, in contrast to the other two terms.

The populations of the ``core" shells p_i in equation (8) have been taken as in [Kr], [Ar] and [He] for yttrium, titanium and oxygen atoms, respectively. The radial function is expanded over Slater functions for each shell. The radial function parameters p_k, ζ_k can be found in (Clementi & Roetti, 1974).

The ``valence'' orbitals have been chosen for each atom as 4d, 5s for yttrium, 3d, 4s for titanium and 2s, 2p for oxygen using Slater type radial functions of ``valence'' orbitals (Clementi & Roetti, 1974). The refined parameters are: the linear combination coefficients ($c_{i\mu}$), the spin-dependent partial orbitals populations ($n_i^{\uparrow}$, $n_i^{\downarrow}$) and the expansion contraction coefficient (κ), which modulates the radial function of valence orbital shells (in equation (6) and (7)).

The refinement was first carried out without the ``bond'' term. The ``bond'' terms which account for titanium-oxygen and yttrium-oxygen couplings were modeled in a second stage; O----O couplings were neglected. As explained above, GTO expansions were used to describe the STO radial functions only for this bond contribution. The expansion parameters are defined as the best approximation of the corresponding radial function of ``valence'' orbitals. The comparison of the radial functions for ``valence'' orbitals and ``bond'' term is shown in figure S1 in supplementary material together with the expansion parameters (tables S1-S3 of supplementary material).

The positions of atoms and their harmonic Debye-Waller factors were simultaneously refined for XRD and PND data using UNIT weighting scheme. For a discussion on the weighting scheme see (Deutsch, et al., 2012). For X-ray data, anharmonicity effects have been taken into account (Gram-Charlier expansion) as in our previous work (Voufack, et al., 2019).

3.3. Agreement factors

The experimental data were described in the framework of two different atomic orbital models, including or not the ``bond'' term. In order to assess the quality of the refinements a comparison with the widely used multipole model is given. The statistical agreement factors for multipole and orbital models are provided in table 1. The agreement factors and goodness-of-fit for all models have similar values. In all cases, the agreement factors $R_w(|F_{charge}|)$ for XRD data are lower than 1.5% showing a very reliable description of electron density. The agreement factors for PND data are higher, which is typical for spin density analysis where weighted agreement factors $R_w(|R-1|)$ usually amount to 10%.

Table 1 Statistical agreement factors for joint refinement procedure of XRD and PND data in the framework of the multipole model, the atomic-orbital model without the ``bond'' term (orbital I) and with the ``bond'' term (orbital II). The spherical atom model is given for comparison. Agreement factors are calculated on $|F_{charge}|$ and $|R-1|$ for XRD and PND data, respectively.

Parameters	multipole	orbital I	orbital II	spherical	data
$R(\%)$	1.40	1.39	1.39	1.47	XRD

$wR(\%)$	1.12	1.12	1.11	1.27	N_{hkl} = 4521
$\sqrt{\chi^2/N_{hkl}}$	1.18	1.18	1.18	1.34	
$R(\%)$	17.21	19.47	19.47	57.83	PND
$wR(\%)$	8.84	9.21	9.20	29.55	N_{hkl} = 291
$\sqrt{\chi^2/N_{hkl}}$	4.14	4.31	4.31	13.8	

The X-rays goodness-of-fits for reflections grouped in 0.1 Å^{-1} range of $\sin\theta/\lambda$ clearly show only very tiny differences in data description by the multipole and orbital models (figure 2). The orbital model yields larger values of χ^2_{XRD} and χ^2_{PND} than the multipole model, as the latter has higher flexibility (ie a higher number of parameters). The distribution of reflections over $\sin\theta/\lambda$ is shown on the same figure by a histogram. Small discrepancies between the two models lie in the sinθ/λ range [0.2 -0.35 Å^{-1}] as it corresponds to the largest d electron scattering (see figure 3). The description of the high-order experimental X-ray data ($\sin\theta/\lambda$>0.8 Å^{-1}) is independent of the model used. The refinement of atomic positions and Debye-Waller factors has the strongest influence on the intensity of high-order reflections, which are found to be similar for the multipole and orbital models (tables S4-S6 in supplementary material). In conclusion, on the sole basis of least-square statistical indices, it is not possible to decide which model is the best. The orbital model describes experimental data with smaller number of physically meaningful parameters than the multipole model.

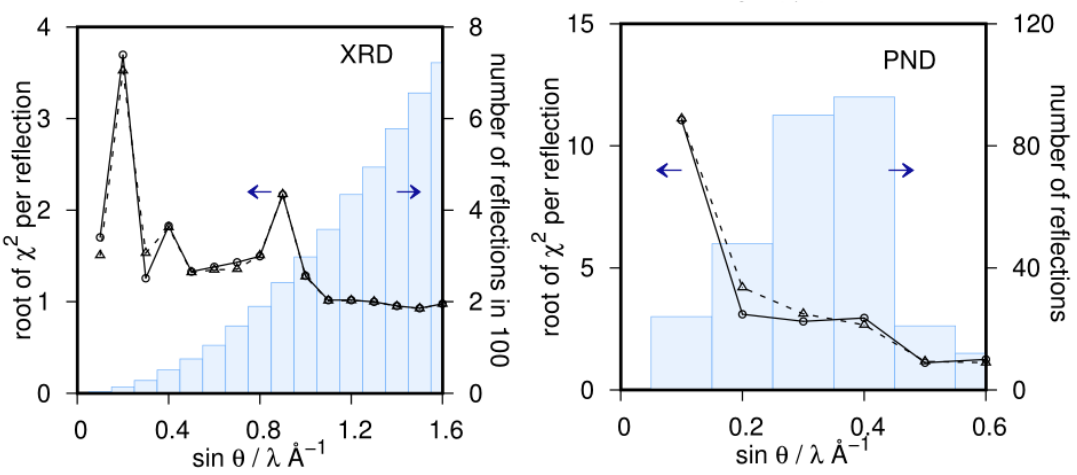

Figure 2 The goodness-of-fit of reflections grouped in 0.1 Å^{-1} ranges of $\sin\theta/\lambda$ (XRD and PND) for multipole (circles with solid line) and orbital models without the ``bond" term (triangles with dotted line). The histogram shows a distribution of reflections (in hundreds for XRD) over $\sin\theta/\lambda$.

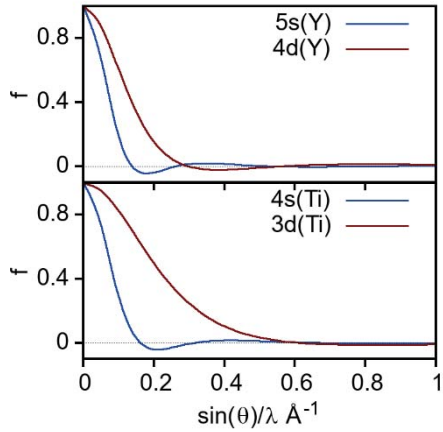

Figure 3 Normalized valence scattering factors 5s and 4d of Y (top) and 4s and 3d of Ti (bottom).

The introduction of ``bond'' terms slightly improves the description of the low-order reflections (see figure S3 in supplementary material). The small contribution of the ``bond'' terms is related to the small covalent contribution between the Ti and O atoms. We expect the impact of "bond" terms to be more visible for a crystal-like pyrite or a molecular crystal where covalency is the leading term. In the present paper we then decided to discuss the atomic orbital model where the ``bond'' term is excluded (model I).

Model I and model II show similar residual densities as the multipolar model. In all cases, the largest residual charge densities are observed around the titanium and yttrium atoms. Most undescribed residual density is directed along the [100] direction (dotted lines on figure 4). We suppose that this noise is due to insufficient absorption corrections for XRD data. It is a common problem when the studied sample has a complex shape. Any uncertainty in the correction increases the residual density around the most significant scatterers along the same direction.

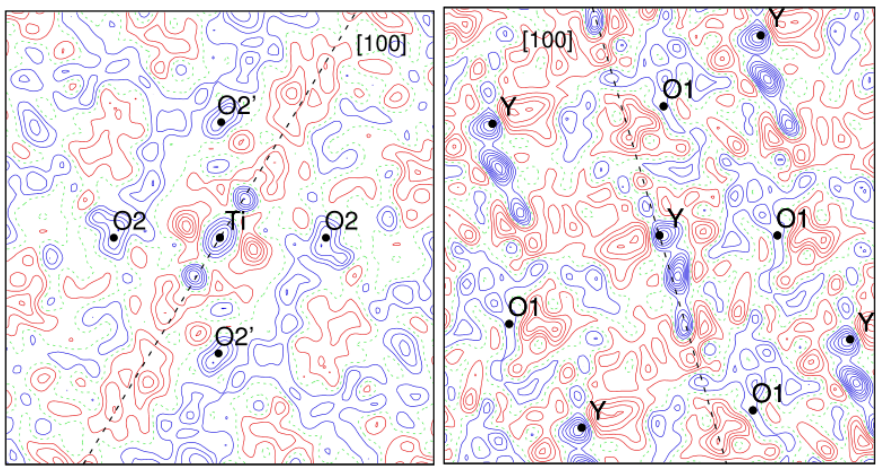

Figure 4 Residual charge density around titanium and yttrium atoms. Contours are 0.10 e/Å^3. Green dotted contours are zero level, red ones are negative, blue ones are positive. The [100] direction is shown by black dotted lines. $\sin(\theta)/\lambda < 1.2\text{Å}^{-1}$.

The residual charge density has a random distribution in the other planes (see figure S4 in supplementary material) proving that the atomic-orbital model correctly describes the experimental data. Note that the residual density is larger in the Y-O_1-O_1 plane as it is a mirror plane.

3.4. Spin-resolved electron density analysis

XRD is highly sensitive to the radial distribution of atomic orbitals. It allows an estimation of their size via the expansion contraction coefficient. The κ parameters of Y and Ti atoms ``valence" orbitals ($4d$ for yttrium and$4s$, $3d$ for titanium) are far from unity (see table 2). This corresponds to the shrinking of outer electronic orbitals, as yttrium and titanium are giving away their electrons to oxygen atoms. Opposite changes are found for oxygen atoms where the p-shell κ parameter is less than one. Thus, the O electronic orbitals are more diffuse compared to the neutral atom as oxygen accepts additional electrons coming from titanium and yttrium.

The ``valence" charge and spin populations of all atoms are summarized in table 2 together with the expansion coefficients $\kappa$ of the ``valence" orbitals. The formal number of electrons on the ``valence" orbitals for neutral and fully ionized atoms is also reported. Clearly the estimated net atomic charges have intermediate values between neutral and fully ionized states, which is a typical situation in charge density analysis. However, the Ti and O net charges obtained by the wave function model I largely differ from those obtained using the multipole model: the titanium is more positively charged (1.5+) giving more electrons to the O1 and O2 atoms (1.0-) in model I. It is in line with the expansion contraction coefficients as the wave function models give larger κ than the multipole ones (table2). It can be noted that the charges obtained from model I (and model II) are very close to those calculated by integration over Bader atomic basins (“Atoms in molecules” (Bader, 1990)) (respectively +1.47 and -1.05); probably due to small covalency in this perovskite.

The total magnetization per titanium atom is 0.90(1) μ_B.The unpaired electron is mostly localized on the titanium atom. The obtained magnetic moments are in line with those calculated from the multipole model. Small magnetic moments previously observed on Y and O_1 (Voufack, et al., 2019; Kibalin, et al., 2017), are in the order of one sigma in the present study. In this model the estimated error bars are significantly larger than the parameter value for Y and O_1. It is a consequence of the contribution of errors from both XRD and PND experiments but also of the large correlation between the parameters of atomic orbitals used for the charge and spin density analysis.

Table 2 Valence and spin populations of ``valence" term. $\kappa_1$ and $\kappa_2$ are the radial expansion contraction factors for 5s, 4s, 2s and 4d, 3d, 2p shells of Y, Ti, O, respectively. The last two columns are the number of electrons on ``valence" orbitals for neutral and fully ionized atoms, respectively.

When no error bar is given, the parameter was fixed during the refinement procedure. These values are compared to those obtained from the joint refinement multipole model (*) and Bader integration (Voufack, et al., 2019) (**)

atom	Pval	Net charge	spin	κ_1	κ_2	neutral	ion
Y	1.4(5)	1.6(5)	0.0(5)	1.0	1.54(2)	3	0
Y*	1.53(7)	1.47(7)	-0.03(7)	1.03(8)	1.49(6)		
Y**		1.80	0.066				
Ti	2.47(8)	1.53(8)	1.05(8)	1.535(4)	1.196(2)	4	1
Ti*	3.40(6)	0.60(6)	1.04(6)	1.14(2)	0.90(3)		
Ti**		1.47	0.628				
O1	6.95(9)	-0.95(9)	0.00(9)	1.0	0.934(1)	6	8
O1*	6.66(3)	-0.66(3)	0.02(3)	0.964(4)	0.88(7)		
O1**		-1.06	0.112				
O2	7.07(7)	-1.07(7)	-0.05(7)	1.0	0.921(1)	6	8
O2*	6.70(2)	-0.70(2)	0.00(2)	0.968(2)	0.98(7)		
O2**		-1.05	0.097				

The redistribution of electrons in comparison with non-interacting neutral IAM atoms is shown on the static charge deformation density (figure 5). The negative difference density around titanium is directed towards the positive distribution around the oxygen atoms: the depopulation of titanium e_g orbitals faces the oxygen p-filled orbitals. Titanium t_{2g} orbitals are more populated than those of the isolated neutral atom (blue contours around titanium in figure 5).

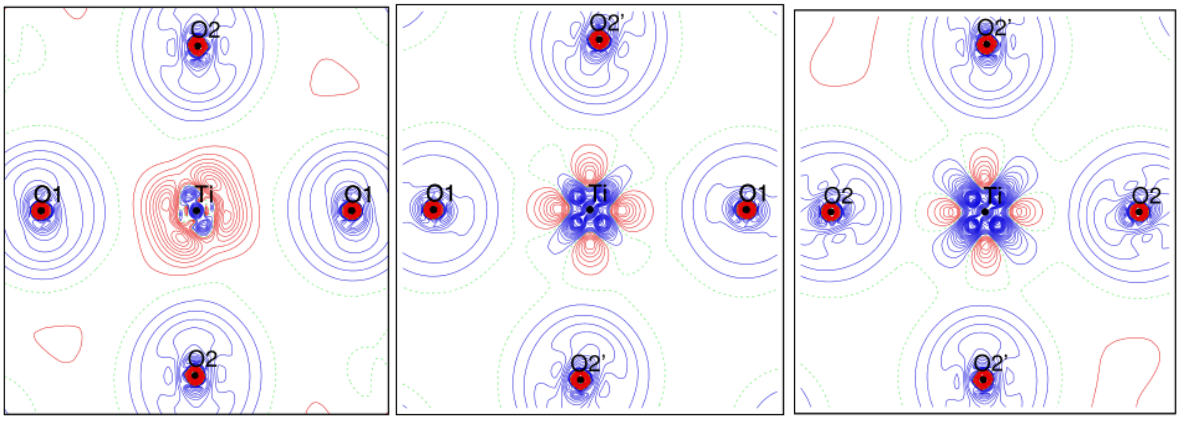

Figure 5 Static charge deformation density around the titanium atom in the xy, xz and yz planes of Ti octahedron. Contours level are 0.05 e/Å^3: green dotted contours are zero level, red ones are negative, blue ones are positive

The orientations and populations of atomic orbitals of titanium are given in table 3. A first remark is that the standard deviations obtained on the wave functions coefficients are large for ϕ_3 ϕ_4, ϕ_5 and ϕ_6 ; very few refined coefficients are statistically non zero. Orbitals ϕ_4, ϕ_5 and ϕ_6 are oriented mostly towards the ligands and are less populated.

The spin density distribution of the titanium, $n_i^{\uparrow}$ and $n_i^{\downarrow}$ shows that the spin up contribution mostly originates from the electrons located on two atomic orbitals ϕ_1 and ϕ_2 when the spin down electrons arise from ϕ_5 and ϕ_3 (mostly $|xy\rangle$). The resulting magnetic moment is due to the $|4s\rangle$ orbital and to the linear combinations of $|zx\rangle$ and $|yz\rangle$ basis orbitals. The orientation coefficients of orbital ϕ_2 are not surprising and are in line with (Akimitsu, et al., 2001). It agrees with our previous work as the multipole model refinement also showed a high spherical contribution to the magnetic moment localized on titanium atom (Voufack, 2018).

Table 3 Linear combination coefficients of the basis functions and populations of ``valence" atomic orbitals of titanium atom.

	ϕ_1	ϕ_2	ϕ_3	ϕ_4	ϕ_5	ϕ_6
$\|4s\rangle$	1	0	0	0	0	0
$\|3d_{z^2}\rangle$	0	-0.03(1)	-0.2(1)	-0.5(2)	0.22(8)	-0.8(2)
$\|3d_{zx}\rangle$	0	0.62(1)	-0.2(3)	-0.34(5)	-0.67(8)	0.1(1)
$\|3d_{yz}\rangle$	0	0.78(1)	0.3(3)	0.19(6)	0.53(9)	-0.07(9)
$\|3d_{x^2y^2}\rangle$	0	0.02(1)	-0.5(2)	-0.5(1)	0.5(2)	0.5(2)
$\|3d_{xy}\rangle$	0	-0.09(1)	0.76(3)	-0.63(4)	0.0(3)	0.1(2)
$n_i^{\uparrow}$	0.60(5)	0.83(1)	0.02(1)	0.18(1)	0.01(1)	0.12(1)
	0.14(5)	-0.01(1)	0.16(1)	0.11(1)	0.22(1)	0.09(1)

The model 3D spin-density distribution in the unit cell is presented in figure 6. The contribution of the aspherical orbital ϕ_2 of titanium to spin density is clearly visible. The spherical contribution of orbital $\phi_1$is not visible on figure 6 as the maximal density localized on the center of titanium decreases quadratically with increasing distance from titanium. The presence of some regions with very weak negative spin distribution could be linked to artifacts in experimental data.

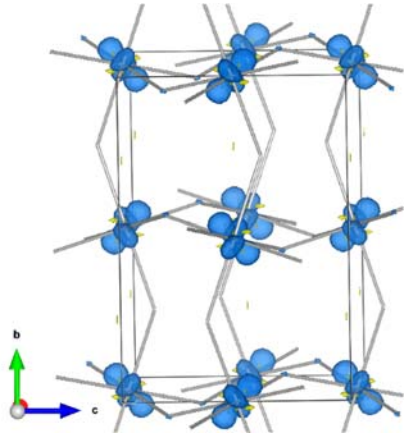

Figure 6 Spin density distribution. Isosurface is 0.40 e/Å^2 (blue is positive, yellow is negative).

Detailed information about population and orientation of atomic orbitals of the ``valence" shell for yttrium and oxygen atoms is given in tables S7-S9. Figure 7 presents the Yttrium static charge deformation density in the (010) plane. The $|5s\rangle$ electrons are redistributed between the$|4d\rangle$ orbital of yttrium and the p-orbital of O_1 facing Y. This is also in agreement with the multipole model.

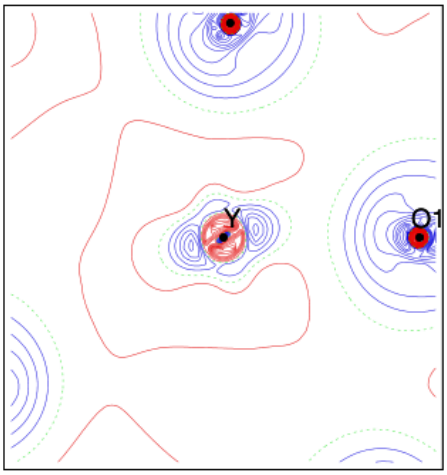

Figure 7 Static charge deformation density on the yttrium atom in the (010) plane. Contour level is 0.05 e/Å^3, red contours are negative, blue contours are positive, dotted green is zero.

4. Conclusion

We have shown that the spin-resolved atomic-orbital model is a reliable tool for analyzing charge and spin electron densities. It allows the characterization of the radial extension of atomic orbitals and directly provides their orientation and population. The atomic orbital and multipolar models are statistically equivalent to describe the electronic structure from experimental data.

When applied to the $YTiO_3$ perovskite, the atomic orbital model confirms the origin of the spin density which is mainly located on the titanium atom. It evidences that not only t_{2g} orbitals are responsible for the magnetic moment but also the $|4s\rangle$ orbital of the titanium atom. The contribution

of other orbitals to the magnetic moment is significantly weaker. For this mostly ionic crystal, the obtained net charges are close to the integrated charges over the Bader atomic basins.

Introducing ``bond'' terms did not statistically improve the data refinement as $YTiO_3$ is mostly ionic. No significant spin contribution arising from the O1 atom was found contrary to the results obtained from the PND and XMD data analysis (Kibalin, et al., 2017).

References

Akimitsu, J. et al., 2001. Direct Observation of Orbital Ordering in $YTiO_3$ by Means of the Polarized Neutron Diffraction Technique. *J. Phys. Soc. Jpn.,* Volume 70, pp. 3475-3478.

Avery, J. & Watson, K. J., 1977. Generalized X-ray scattering factors. Simple closed-form expressions for the one-centre case with Slater-type orbitals. *Acta Cryst.,* Volume A33, pp. 679-680.

Bader, R. W., 1990. *Atoms in Molecules - A Quantum Theory.* Oxford: Oxford University Press.

Bentley, J., Stewart, R. & Anon.,, 1973. Two-center calculations for X-ray scattering. *Journal of Computational Physics,* 11(1), pp. 127-145.

Bonham, R., 1965. The Evaluation of Two Center Integrals Involved in the Calculation of the Intensity of Diffracted Electrons and X-Rays from Molecules. *J. Phys. Soc. Jpn.,* Volume 20, pp. 2260-2262.

Brown, P. J., Capiomont, A., Gillon, B. & Schweizer, J., 1979. Spin densities in free radicals. *Journal of Magnetism and Magnetic Materials,* Volume 14, pp. 289-294.

Bytheway, I., Figgis, B. N. & Sobolev, A. N., 2001. Charge density in Cu(glygly)(OH2)2·H2O at 10 K and the reproducibility of atomic orbital populations. *J. Chem. Soc., Dalton Trans.,* Volume 22, pp. 3285-3294.

Chandler, G. S. & Spackman, M. A., 1978. Fourier transforms of Gaussian orbital products. *Acta Cryst.,* Volume A34, pp. 341-343.

Clementi, E. & Roetti, C., 1974. Roothaan-Hartree-Fock atomic wavefunctions: Basis functions and their coefficients for ground and certain excited states of neutral and ionized atoms, Z≤54. *Atomic Data and Nuclear Data Tables,* 14(3-4), pp. 177-478.

Deutsch, M. et al., 2012. Experimental determination of spin-dependent electron density by joint refinement of X-ray and polarized neutron diffraction data. *Acta Cryst.,* Volume A68, pp. 675-686.

Deutsch, M. et al., 2014. First spin-resolved electron distributions in crystals from combined polarized neutron and X-ray diffraction experiments. *IUCrJ,* 1(3), pp. 194-199.

Gillon, B. & Becker, P., 2011. Magnetization Densities in Material Science. In: *Modern Charge-Density Analysis.* Dordrecht: Springer, Dordrecht, pp. 277-302.

Hamilton, W., 1964. *Statistical Methods in the Physical Sciences.* Ronald Press: New York.

Hansen, N. K. & Coppens, P., 1978. Testing aspherical atom refinements on small-molecule data sets. *Acta Cryst.,* Volume A34, pp. 909-921.

Hester, J. R. et al., 1997. Electron Density in YTiO3. *Acta Cryst.,* Volume B53, pp. 739-744.

Holladay, A., Leung, P. & Coppens, P., 1983. Generalized relations between d-orbital occupancies of transition-metal atoms and electron-density multipole population parameters from X-ray diffraction data. *Acta Cryst.,* Volume A39, pp. 377-387.

Iga, F. et al., 2004. Determination of the Orbital Polarization in YTiO3 by Using Soft X-Ray Linear Dichroism. *Phys. Rev. Lett.,* Volume 93, p. 257207.

Itoh, M. & Tsuchiya, M., 2001. Orbital ordering in YTiO3 observed by NMR. *Journal of Magnetism and Magnetic Materials,* Volume 226, pp. 874-875.

Ito, M. et al., 2004. Observation of ordered orbital of YTIO3 by the X-ray magnetic diffraction experiments. *Journal of Physics and Chemistry of Solids,* 65(12), pp. 1993-1997.

Jelsch, C., Guillot, B., Lagoutte, A. & Lecomte, C., 2005. Advances in protein and small-molecule charge-density refinement methods using MoPro. *J. Appl. Cryst.,* Volume 38, pp. 38-54.

Kibalin, I. A. et al., 2017. Spin density in YTiO3: I. Joint refinement of polarized neutron diffraction and magnetic x-ray diffraction data leading to insights into orbital ordering. *Phys. Rev. B,* Volume 96, p. 054426.

Li, B. et al., 2014. Dynamic Distortions in the YTiO3 Ferromagnet. *J. Phys. Soc. Jpn.,* Volume 83, p. 084601.

Mochizuki, M. & Imada, M., 2004. Orbital physics in the perovskite Ti oxides. *New Journal of Physics,* Volume 6, pp. 154-154.

Nakao, H. et al., 2002. Quantitative determination of the atomic scattering tensor in orbitally ordered YTiO3 by using a resonant x-ray scattering technique. *Phys. Rev. B,* Volume 66, p. 184419.

Niehaus, T. A., López, R. & Rico, J. F., 2008. Efficient evaluation of the Fourier transform over products of Slater-type orbitals on different centers. *Journal of Physics A: Mathematical and Theoretical,* Volume 41, p. 485205.

Raymond, K. N., 1972. Application of constraints to derivatives in least-squares refinement. *Acta Cryst.,* Volume A28, pp. 163-166.

Schuchardt, K. et al., 2007. Basis Set Exchange: A Community Database for Computational Sciences. *J. Chem. Inf. Model.,* 47(3), pp. 1045-1052.

Schweizer, J. & Ressouche, E., 2001. In: *MagnetoScience – From Molecules to Materials.* s.l.:Wiley, pp. 325-357.

Shmueli, U., 2001. *International Tables for Crystallography.* Oxford: Alden Press.

Stewart, R. F., 1969. Generalized X-Ray Scattering Factors. *The Journal of Chemical Physics,* Volume 51, p. 4569.

Stewart, R. F., Davidson, E. R. & Simpson, W. T., 1965. Coherent X-Ray Scattering for the Hydrogen Atom in the Hydrogen Molecule. *J. Chem. Phys.,* Volume 42, p. 3175.

Tanaka K., 1993. X-ray analysis of wavefunctions by the least-squares method incorporating orthonormality. II. Ground state of the Cu^{2+} ion of bis(1,5-diazacyclooctane)copper(II) nitrate in a low-symmetry crystal field. *Acta Cryst.,* Volume B49, pp. 1001-1010.

Tanaka, K., 1988. X-ray analysis of wavefunctions by the least-squares method incorporating orthonormality. I. General formalism. *Acta Cryst.,* Volume A44, pp. 1002-1008.

Tsuji, N. et al., 2008. Magnetic Compton Profile Study of Orbital Ordering State of 3d Electrons in YTiO3. *J. Phys. Soc. Jpn.,* Volume 77, p. 023705.

Ulrich, C. et al., 2002. Magnetic Order and Dynamics in an Orbitally Degenerate Ferromagnetic Insulator. *Phys. Rev. Lett.,* Volume 89, p. 167202.

Voufack, A. B., 2018. *PhD Thesis.* Nancy: CRM2 Université de Lorraine.

Voufack, A. B. et al., 2017. When combined X-ray and polarized neutron diffraction data challenge high-level calculations: spin-resolved electron density of an organic radical. *Acta Cryst.,* Volume B73, pp. 544-549.

Voufack, A. B. et al., 2019. Spin resolved electron density study of $YTiO_3$ in its ferromagnetic phase: signature of orbital ordering. *IUCrJ,* 6(5), pp. 884-894.

Vuković, T. & Dmitrović, S., 2010. Extremely compact formulas for the Fourier transform of a product of two-centre Slater-type orbitals. *Journal of Physics A: Mathematical and Theoretical,* Volume 43, p. 455208.

Appendix A. Modified Hamilton method

The Hamilton method was modified to apply linear and non-linear constraints during the least-squares refinement procedure. The constraints on the refined parameters, described in section 2D, can be written in a vector form with the equality:

$$\vec{C}(\vec{p}) = \vec{0}, \tag{15}$$

where $\vec{p}$ is the vector of model parameters, $\vec{C}$ is the vector of constrained functions.

In the classical Hamilton method (Hamilton, 1964) the change of the model parameters $\Delta\vec{p}_{new}$, which satisfies the linear constraints, is calculated as:

$$\Delta\vec{p}_{new} = \Delta\vec{p} - \Delta\vec{p} \cdot Q^T\left(QH_{\vec{p}}^{-1}Q^T\right)^{-1}QH_{\vec{p}}^{-1}, \tag{16}$$

where $H_{\vec{p}}$is the Hessian over χ^2, $\Delta\vec{p}$ is the shift of model parameters without any restrictions on the refined parameters. The constraint matrix Q is estimated as

$$Q_{ij} = \left\{ \left. \frac{\partial C_i}{\partial p_j} \right|_{\vec{p}_{new}} \right\}. \quad (17)$$

For linear type of constraints, the matrix Q is constant for any model parameter $\vec{p}$. Therefore, the derivatives calculated at the starting point $\vec{p}_0$ are equal to the derivatives calculated at the final point $\vec{p}_{new}$. For a non-linear type of constraints, the solution of equation (16) taking into account (17) has to be found.

The solution can be established by applying an iterative procedure. The model parameters shift calculated in the previous iteration $\Delta\vec{p}_n$ is used for estimating the matrix Q_n with the subsequent calculation of the shift of the model parameters for the next iteration $\Delta\vec{p}_{n+1}$:

$$Q_n = \left\{ \left. \frac{\partial C_i}{\partial p_j} \right|_{\vec{p}_n} \right\}, \quad (18)$$

$$\Delta\vec{p}_{n+1} = \Delta\vec{p}_n - \Delta\vec{p}_n Q_n^T \left(Q_n H_{\vec{p}}^{-1} Q_n^T\right)^{-1} Q_n H_{\vec{p}}^{-1}, \quad (19)$$

$$\vec{p}_{n+1} = \vec{p}_n + \Delta\vec{p}_{n+1}. \quad (20)$$

This procedure works well with linear and non-linear types of constraints. It has been introduced into the `` MOLLYNX'' program (Deutsch, et al., 2012) to perform the least-squares refinement procedure under constraint conditions.

Supporting information

S1. Representation of radial functions through expansion over Gaussian functions for titanium, yttrium and oxygen

The expansion parameters of GTO functions (eq. 7) which is used to describe the STO radial function of "valence" orbitals for titanium, yttrium and oxygen is presented in tables S1, S2, S3. The comparison of the radial functions described by STO and GTO functions for "valence" orbitals is presented on the figure S1 for corresponding atoms.

Table S1 "Valence" orbitals for titanium. Representation through Gaussian functions.

p_k (4S)	α_k (4s)	p_k (3d)	α_k (3d)
0.41318	0.10263	0.05680	0.26736
0.71920	0.26404	0.22987	0.74234
-0.47347	2.43669	0.40659	1.87259
-0.05144	17.56035	0.38758	5.10434
0.19515	28.28142	0.20989	14.17314
-0.02649	160.61295	0.05842	45.53364
		0.00735	184.02337

Table S2 "Valence" orbitals for yttrium. Representation through Gaussian functions.

p_k (5S)	α_k (5s)	p_k (4d)	α_k (4d)
0.35633	0.08021	0.02963	0.11163
0.79646	0.19808	0.17752	0.25542
-0.58090	1.66969	0.35183	0.58039
0.23182	15.36098	0.40549	1.34636
-0.09107	83.01756	0.27202	3.30473
-0.04154	2613.08849	-0.12671	27.15014
5.10332	3875.85660	-0.06503	91.91714
-6.52741	4007.46230	-0.00953	392.73275
1.48242	4419.97899		

Table S3 "Valence" orbitals for oxygen. Representation through Gaussian functions.

p_k (2S)	α_k (2s)	p_k (2p)	α_k (2p)
0.12234	0.54255	0.10074	0.39333
0.49402	1.33715	0.38465	1.14864
0.49227	3.45871	0.45020	3.42993
-0.25281	35.56531	0.25703	11.03848
0.26109	146.98360	0.06450	42.45348
-0.35469	154.77130	0.00675	237.74589
-0.01208	1854.08720		

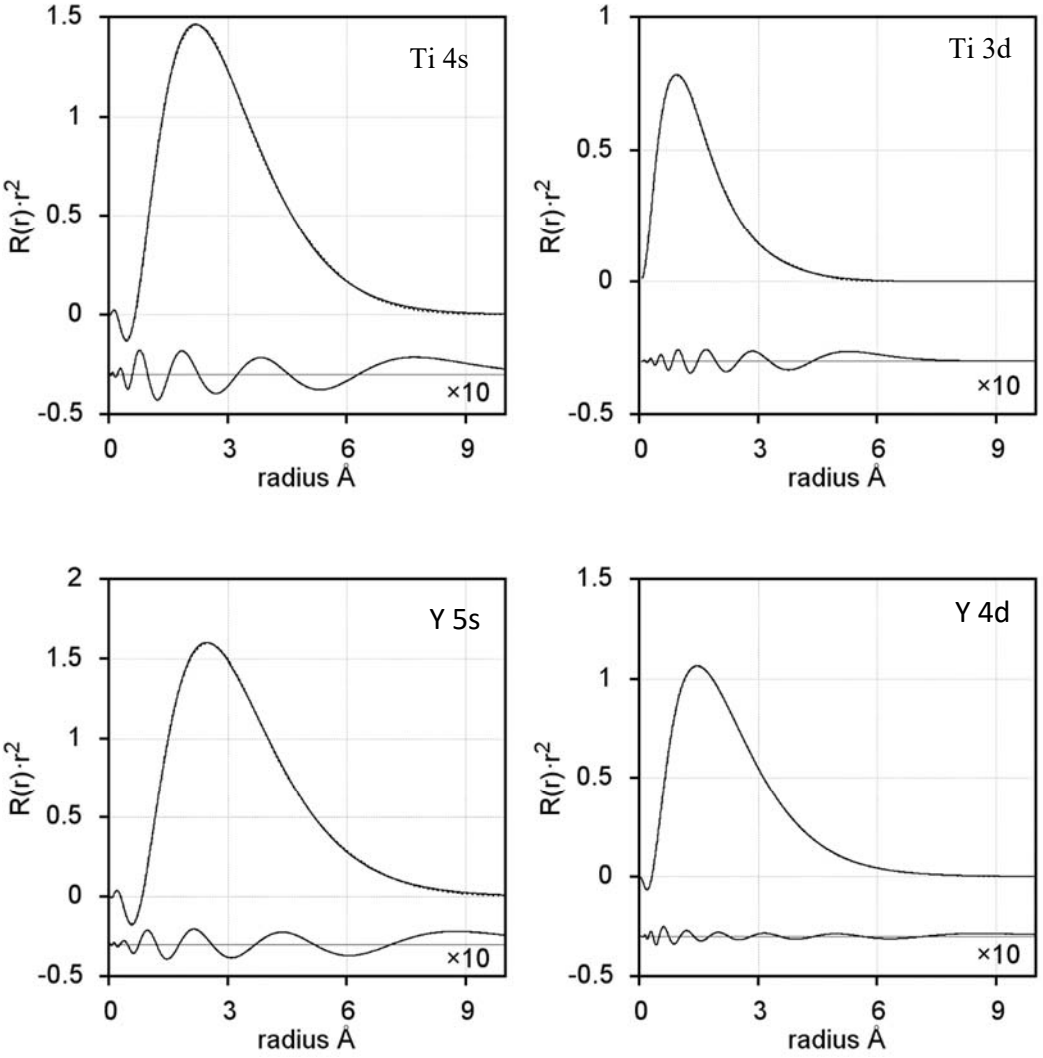

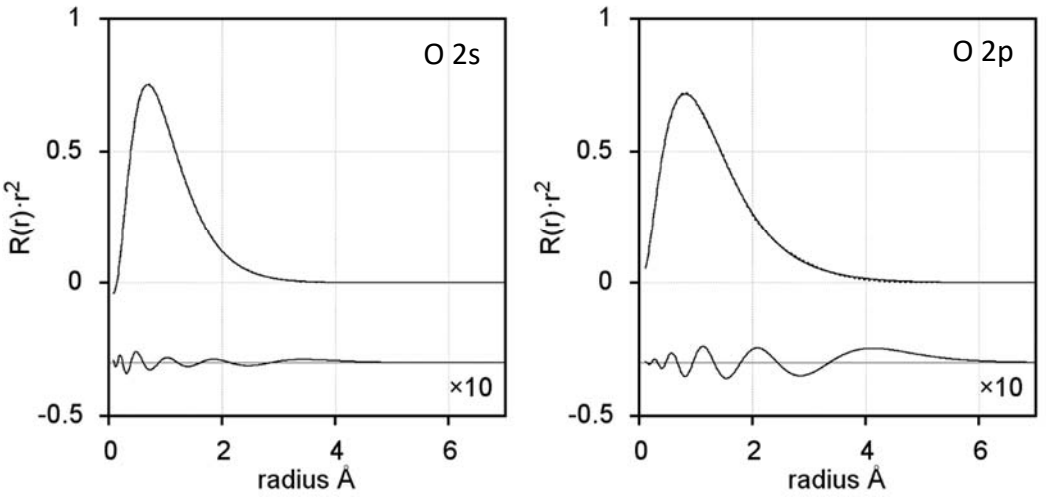

Figure S1 Radial function weighted on r^2 expressed through Slater (solid line) and Gaussian functions (dotted line) for titanium, yttrium and oxygen. Multiplied by ten the difference between models is shown below.

S2. Refinement in frame of orbital and multipole models

The figure S2 shows the definition of local Cartesian coordinate system for each atom in asymmetric unit cell. Y has axis "Y" to O1 (closest), axis "Z" along "b" axis; Ti has axis "Z" to O_2 (more distant), axis "X" to O_1 ; O_1 has axis "X" to Y (closest), axis "Z" along "b"; O_2 has axis "X" to Ti (more distant), axis "Y" to O_1.

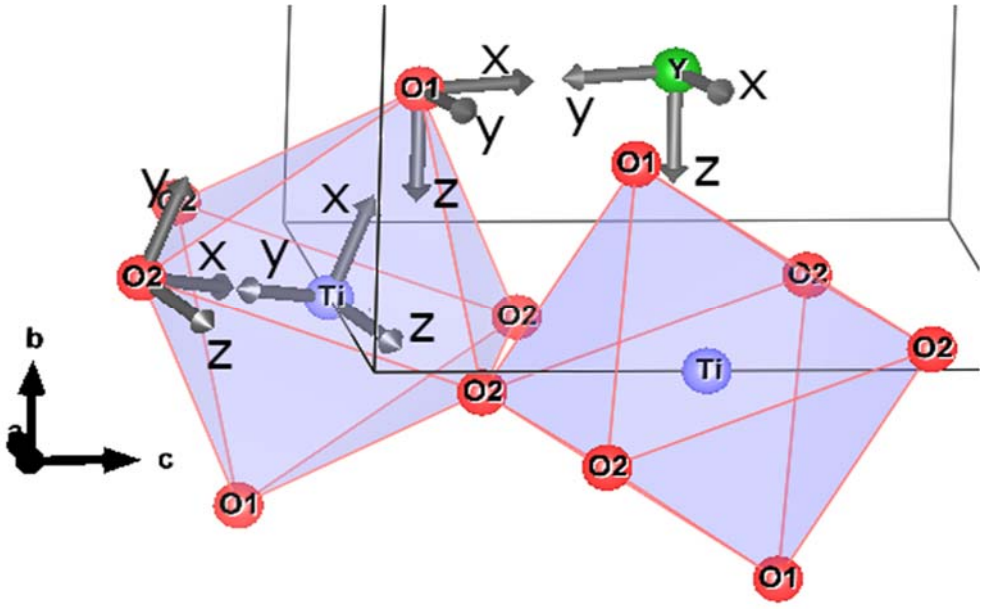

Figure S2 Definition of Cartesian local coordinate system for each atom in asymmetric unit cell.

Table S4 Coordinates and harmonic vibration parameters for each atom after refinement in frame of multipole and orbital models.

	Multipole model			
	Ti	Y	O_1	O_2
x	0.5	0.574144(3)	0.457507(26)	0.309438(18)
y	0.0	0.25	0.25	0.057899(14)
z	0.0	0.522086(3)	0.121074(29)	-0.309518(20)
U_{11}, Å	0.001994(9)	0.001883(5)	0.003884(33)	0.003632(25)
U_{22}, Å	0.001444(8)	0.002137(4)	0.002624(32)	0.004072(25)
U_{33}, Å	0.002498(7)	0.002112(4)	0.003743(37)	0.003676(26)
U_{12}, Å	-0.000120(6)	0	0	-0.000622(20)
U_{13}, Å	-0.000157(6)	0.000064(3)	-0.000633(28)	-0.000627(19)
U_{23}, Å	-0.000005(5)	0	0	0.000430(20)
	Orbital model			
	Ti	Y	O_1	O_2
x	0.5	0.574147(3)	0.457512(27)	0.309449(18)
y	0	0.25	0.25	0.057893(14)
z	0	0.522075(4)	0.121029(30)	-0.309529(21)
U_{11}, Å	0.002116(9)	0.001938(5)	0.003845(34)	0.003614(26)
U_{22}, Å	0.001474(8)	0.002007(4)	0.002602(33)	0.004061(26)
U_{33}, Å	0.002401(8)	0.002154(4)	0.003775(38)	0.003650(27)
U_{12}, Å	0.000091(7)	0	0	-0.000613(21)
U_{13}, Å	-0.000059(6)	0.000054(3)	-0.000661(29)	-0.000629(19)
U_{23}, Å	0.000020(6)	0	0	0.000422(21)

Table S5 Parameters of anharmonicity for titanium atom.

4th order (the parameters are multiplied by 10^5)

name	orbital	multipole	name	orbital	multipole	name	orbital	multipole

1111	2(3)	-6(3)	1122	5(5)	-7(5)	1233	-4(10)	-29(10)
2222	1.4(7)	0.9(7)	1123	-8(9)	14(8)	1333	-12(7)	-44(7)
3333	31(3)	43(2)	1133	-11(9)	-2(9)	2223	11(2)	-3(2)
1112	12(6)	-1(5)	1222	9(3)	-15(3)	2233	-8(5)	-2(5)
1113	-1(6)	-26(6)	1223	6(6)	25(6)	2333	4(5)	12(5)

6th order (the parameters are multiplied by 10^5)

name	orbital	multipole	name	orbital	multipole	name	orbital	multipole
111111	-1.0(9)	-2.2(8)	111233	7(5)	2(5)	122333	-4(3)	-1(3)
222222	0.4(1)	0.3(1)	111333	-2(4)	-14(3)	123333	-1(4)	-5(4)
333333	3(1)	5(1)	112222	3(1)	2(1)	133333	-2(3)	-9(3)
111112	3(2)	2(2)	112223	2(2)	3(2)	222223	1.1(4)	0.1(4)
111113	1(2)	-4(2)	112233	-14(4)	-13(4)	222233	-2.5(9)	-1.9(9)
111122	8(2)	5(2)	112333	-3(5)	6(4)	222333	3(1)	2(1)
111123	-3(4)	3(3)	113333	9(4)	14(3)	223333	6(2)	9(2)
111133	5(4)	6(3)	122222	1.3(5)	-1.4(4)	233333	2(2)	4(2)
111222	4(1)	-2(1)	122223	2(1)	5(1)			
111223	4(3)	7(3)	122233	-4(3)	-12(3)			

Table S6 Parameters of anharmonicity for yttrium atom.

3rd order (the parameters are multiplied by 105)

name	orbital	multipole	name	orbital	multipole	name	orbital	multipole
111	9(2)	10(2)	122	37(2)	37(2)	233	0.00	0.00
222	0.00	0.0	113	10(4)	9(4)	123	0.00	0.00
333	-7(2)	-4(2)	133	6(4)	6(4)			
112	0.00	0.0	223	18(2)	18(2)			

4th order (the parameters are multiplied by 10^5)

name	orbital	multipole	name	orbital	multipole	name	orbital	multipole

1111	21(1)	18(1)	1122	16(3)	20(3)	1233	0.00	0.0
2222	4.4(4)	8.6(4)	1123	0.00	0.0	1333	-4(3)	-2(3)
3333	25(2)	24(2)	1133	-9(5)	-29(5)	2223	0.00	0.0
1112	0.00	0.0	1222	0.00	0.0	2233	-4(3)	-4(3)
1113	-4(3)	1(3)	1223	-6(3)	-7(3)	2333	0.00	0.0

5th order (the parameters are multiplied by 10^5)

name	orbital	multipole	name	orbital	multipole	name	orbital	multipole
11111	1.1(5)	1.1(4)	11133	1(1)	1(1)	12233	3(1)	3(1)
22222	0.00	0.0	11222	0.00	0.0	12333	0.00	0.0
33333	-2.9(6)	-2.5(5)	11223	0(1)	0(1)	13333	1(1)	1(1)
11112	0.00	0.0	11233	0.00	0.0	22223	0.7(3)	0.8(3)
11113	4(1)	3(1)	11333	1(1)	1(1)	22233	0.00	0.0
11122	4.1(7)	4.0(7)	12222	3.1(3)	3.1(3)	22333	4.8(8)	5.1(7)
11123	0.00	0.0	12223	0.00	0.0	23333	0.00	0.0

6th order (the parameters are multiplied by 10^5)

name	orbital	multipole	name	orbital	multipole	name	orbital	multipole
111111	3.5(5)	3.1(5)	111233	0.00	0.0	122333	3(2)	2(1)
222222	0.4(1)	0.8(1)	111333	-4(2)	-3(2)	123333	0.00	0.0
333333	3.1(6)	3.3(5)	112222	3.8(5)	4.9(6)	133333	-1(1)	1(1)
111112	0.00	0.0	112223	0.00	0.0	222223	0.00	0.0
111113	0(1)	1(1)	112233	-17(2)	-19(2)	222233	-3.1(5)	-2.6(5)
111122	12.4(9)	12.7(9)	112333	0.00	0.0	222333	0.00	0.0
111123	0.00	0.0	113333	8(2)	3(1)	223333	5(1)	4.9(9)
111133	8(2)	3(2)	122222	0.00	0.0	233333	0.00	0.0
111222	0.00	0.0	122223	-0.8(6)	-1.1(6)			
111223	-4(2)	-4(2)	122233	0.00	0.0			

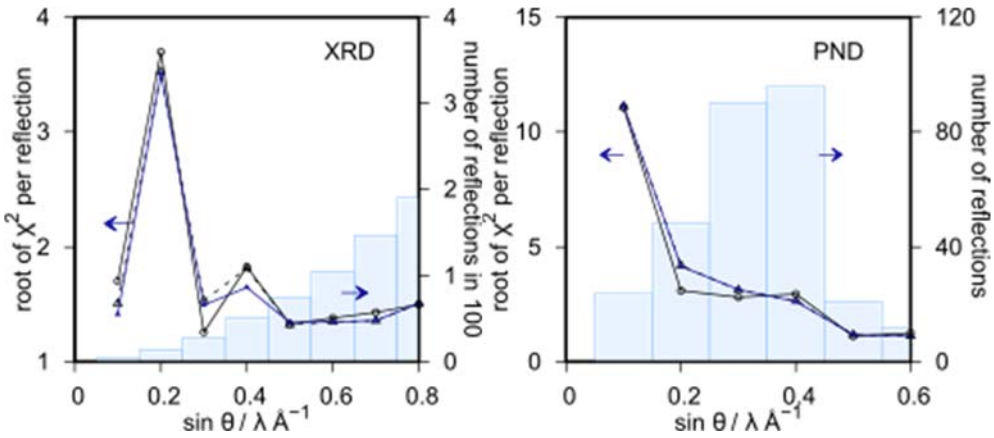

Figure S3 The goodness-of-fit of reflections grouped in 0.1 Å−1 ranges of sinθ/λ (XRD and PND data) for multipole (circles with solid line) and orbital model with and without out "interaction" term (black open and blue closed triangles).

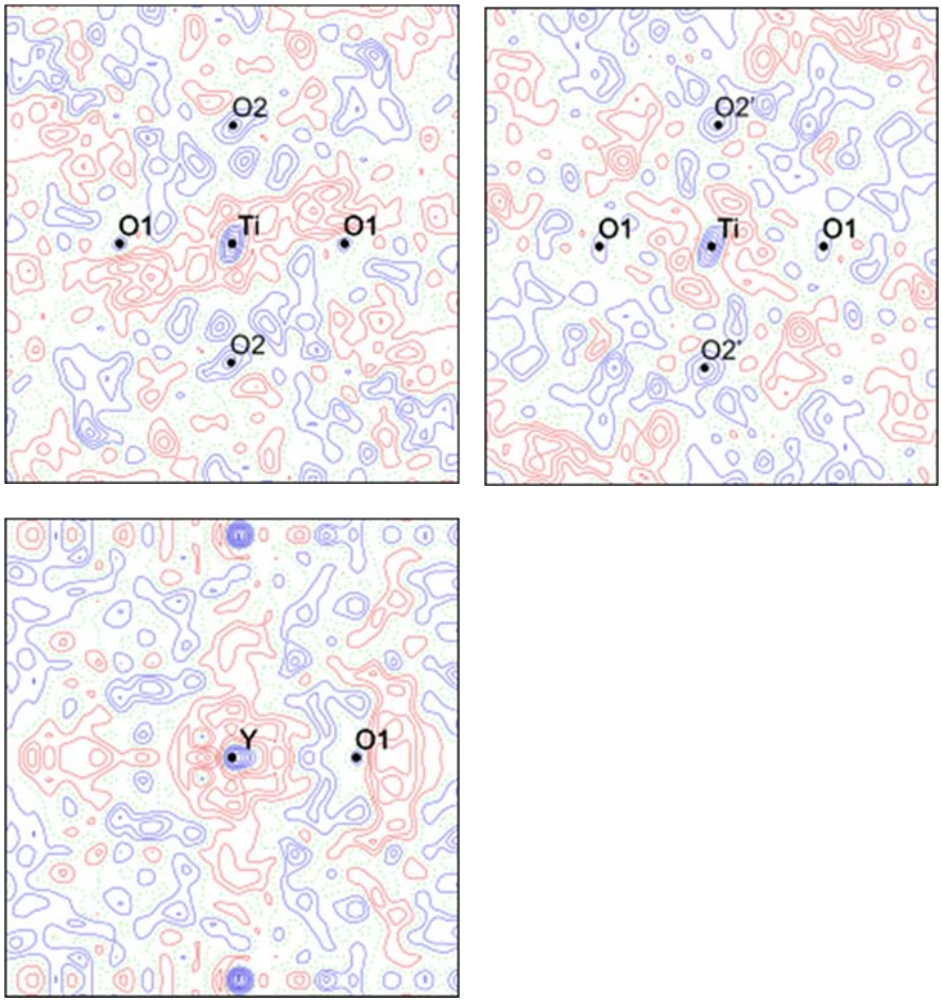

Figure S4 Low-order residual densities around titanium and yttrium atoms Ti-O_1-O_2, Ti-O_1-O_2', Y-O_1-axis "b". Contours are 0.10 el./Å^3. $\sin(\theta)/\lambda < 1.2\text{Å}^{-1}$.

S3. Orientation and population of "valence" atomic orbitals located on Y, O_1, O_2

Table S7 "Valence" atomic orbitals located on yttrium.

	ϕ_1	ϕ_2	ϕ_3	ϕ_4	ϕ_5	ϕ_6
$\|5s\rangle$	0	0	0	0	0	1
$\|4d_{z^2}\rangle$	0	-0.51(3)	0.17(43)	0	0.84(54)	0
$\|4d_{zx}\rangle$	-0.97(10)	0	0	-0.26(4)	0	0
$\|4d_{yz}\rangle$	-0.26(13)	0	0	0.97(2)	0	0
$\|4d_{x^2y^2}\rangle$	0	-0.75(3)	0.39(28)	0	-0.54(74)	0
$\|4d_{xy}\rangle$	0	-0.42(3)	-0.90(13)	0	-0.07(132)	0
$n_i^{\uparrow}$	0.07(2)	0.01(2)	0.04(1)	0.21(2)	0.02(1)	0.40(33)
$n_i^{\downarrow}$	0.07(2)	0.15(2)	0.02(2)	0.10(2)	0.01(2)	0.35(33)
charge	0.14(2)	0.16(3)	0.05(2)	0.32(2)	0.03(2)	0.75(47)
spin	0.00(2)	-0.15(3)	0.02(2)	0.11(2)	0.00(2)	0.05(48)

Table S8 "Valence" atomic orbitals located on oxygen 1.

	ϕ_1	ϕ_2	ϕ_3	ϕ_4
$\|2s\rangle$	1	0	0	0
$\|2p_x\rangle$	0	0.988(5)	-0.15(25)	0
$\|2p_y\rangle$	0	-0.155(25)	-0.988(5)	0
$\|2p_z\rangle$	0	0	0	1.00
$n_i^{\uparrow}$	0.72(5)	0.93(2)	0.92(2)	0.90(2)
$n_i^{\downarrow}$	0.69(5)	0.95(2)	0.89(2)	0.95(2)
charge	1.41(7)	1.88(3)	1.81(3)	1.84(3)
spin	0.04(7)	-0.02(3)	0.04(3)	-0.05(3)

Table S9 "Valence" atomic orbitals located on oxygen 2.

	ϕ_1	ϕ_2	ϕ_3	ϕ_4
$\|2s\rangle$	1	0	0	0
$\|2p_x\rangle$	0	0.95(1)	-0.08(10)	0.31(2)
$\|2p_y\rangle$	0	0.06(9)	1.00(1)	0.07(4)
$\|2p_z\rangle$	0	-0.31(2)	-0.05(4)	0.95(1)
$n_i^{\uparrow}$	0.79(4)	0.93(2)	0.89(2)	0.91(2)
$n_i^{\downarrow}$	0.50(4)	1.07(2)	1.01(2)	0.99(2)
charge	1.29(6)	1.99(2)	1.90(2)	1.90(2)
spin	0.30(6)	-0.14(2)	-0.12(2)	-0.08(2)